

Density of triangulated ternary disc packings

Thomas Fernique^{1,2} and Daria Pchelina²

¹CNRS

²LIPN, Univ. Paris Nord, 93430 Villetaneuse, France

November 8, 2022

Abstract

We consider *ternary* disc packings of the plane, i.e. the packings using discs of three different radii. Packings in which each “hole” is bounded by three pairwise tangent discs are called *triangulated*. There are 164 pairs (r, s) , $1 > r > s$, allowing triangulated packings by discs of radii 1, r and s . In this paper, we enhance existing methods of dealing with maximal-density packings in order to find ternary triangulated packings which maximize the density among all the packings with the same disc radii. We showed for 16 pairs that the density is maximized by a triangulated ternary packing; for 15 other pairs, we proved the density to be maximized by a triangulated packing using only two sizes of discs; for 40 pairs, we found non-triangulated packings strictly denser than any triangulated one; finally, we classified the remaining cases where our methods are not applicable.

1 Density of disc and sphere packings

Given a finite set S of discs, a *packing* of the plane by S is a collection of translated copies of discs from S with disjoint interiors.

Given a packing P , its *density* $\delta(P)$ is the proportion of the plane covered by the discs. More formally,

$$\delta(P) := \limsup_{n \rightarrow \infty} \frac{\text{area}([-n, n]^2 \cap P)}{\text{area}([-n, n]^2)}.$$

Nowadays, the density of disc packings is widely studied in different contexts. The worst-case optimal density of packings in triangular and circular

containers is found in [FMS17, FKS22]. In computer science, there are various connections between sphere packings and error-correcting codes [CS98]. Researchers in chemical physics used Monte Carlo simulations on 2-disc packings and, among others, obtained lower bounds on the maximal density of packings with particular disc sizes [FJFS20]. Two other groups of physicists found lower bounds on maximal densities of packings in \mathbb{R}^3 with 2 sizes of spheres [HST12, OH11]. Upper bounds on the density are usually much harder to obtain.

The main problem we are interested in is the following: given a finite set of ball sizes in \mathbb{R}^2 (or \mathbb{R}^3), find a packing of the plane (or of the space) maximizing the density.

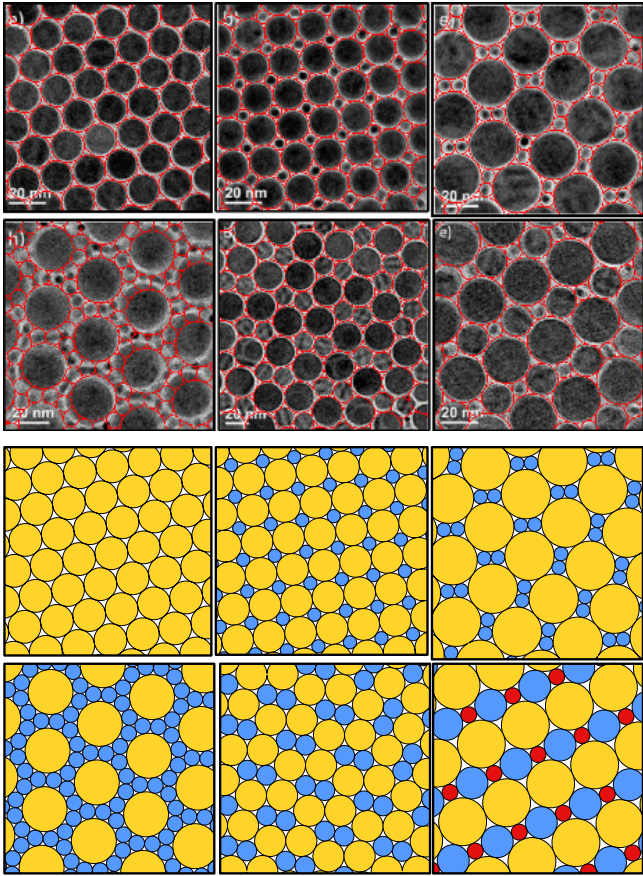


Figure 1: Disc packings self-assembled from colloidal nanodiscs and nanorods in [PDKM15] (at the top) which very accurately correspond to triangulated packings (on the bottom).

Answering this question has a few practical applications. Chemists, for example, are interested in the disc and sphere sizes maximizing the density in order to eventually design compact materials using spherical nanoparticles of given sizes [PDKM15, FJFS20, HST12]. Figure 1 gives an illustration of experimental results from [PDKM15].

The first known studies of the densest packings go back to Kepler. Many advances in this area have been made since then.

1.1 Spheres

In a Kepler manuscript dated by 1611, we find a description of the “cannonball” packing followed by an assertion that it is a densest *1-sphere packings* (i.e. packings by equally sized spheres) of the three-dimensional Euclidean space. This assertion is widely known by name of the Kepler conjecture. The “cannonball” packing, also called face-centered-cubic (FCC) packing, belongs to a family of packings formed by stacking layers of spheres centered in the vertices of a triangular lattice, like it is shown in Figure 2. After placing the first two layers, at each step, there are two choices of how to place the next layer. This gives us an uncountable set of packings having the same density. These packings are called *close-packings* of equal spheres.

Conjecture 1 (Kepler 1611) *The density $\delta(P)$ of packing P of \mathbb{R}^3 by unit spheres never exceeds the density of a close-packing:*

$$\delta(P) \leq \frac{\pi}{3\sqrt{2}}. \quad (1)$$

The first advancement in a proof of the Kepler conjecture was made by Gauss who, in 1831, showed that close sphere packings maximize the density among all possible *lattice* packings, i.e. those where the disc centers form a lattice [Gau31]. However, the proof of the whole conjecture took four centuries to be found. Hilbert included this conjecture, also named “the sphere packing problem”, in his famous list of 23 problems published in 1900.

The Kepler conjecture was finally proved in a series of 6 papers submitted by Hales and Ferguson in 1998 [HF06, Hal05]. Their computer-assisted proof took 8 years to be fully reviewed. In 2003, Hales founded a project called Flyspeck in order to fully verify his proof by an automated theorem prover. Flyspeck was completed in 2014 including the proof of the Kepler conjecture in the list of computer verified proofs [HAB⁺17].

The rough idea of the proof consists of locally redistributing (or weighting) the density function and showing inequality (1) for this redistributed

(weighted) density. Lagarias calls this approach “localization” [Lag02]. All in all, in our work, we use the same general ideas which are discussed in detail in Section 3.1.

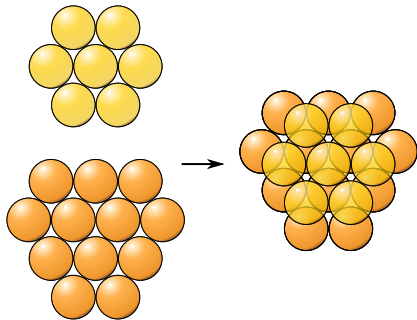


Figure 2: First step of construction of a 3D close-packing.

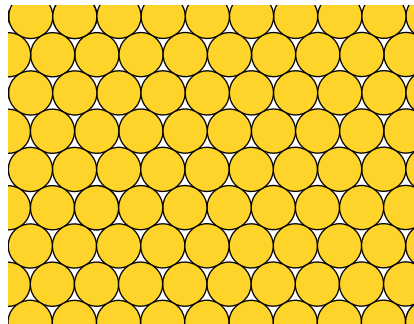


Figure 3: 2D hexagonal packing.

1.2 Discs

1.2.1 1-disc packings

The two-dimensional variant of the Kepler conjecture claims the 2D hexagonal packing on the plane (see Fig. 3) to have the highest density among all planar packings by identical discs.

In 1772, Lagrange proved it to be a densest among lattice packings. The general result was first shown by Thue in 1910 [Thu10]. His proof was however considered incomplete, a reliable proof was given by Fejes-Tóth in 1942 [FT43].

A packing by a set of discs is called *saturated* if no more discs from this set can be added to the packing without intersecting already placed discs. In our setup, we always assume packings to be saturated since we are interested in the upper bounds on the density and adding discs to a packing augments it.

The proof of the two-dimensional Kepler conjecture contains the basics of the strategy used to prove similar results for packings with several disc sizes, like binary packings (discussed in the next section) and ternary packings which are studied in this paper. We thus find it useful to provide the idea of this proof, following its version given in [CW10].

Let P^* denote the hexagonal packing of identical discs of radius 1. Our aim is to show for any saturated two-dimensional packing P using discs of radius 1, that its density does not exceed the density $\delta^* := \frac{\pi}{2\sqrt{3}}$ of P^* .

First, let us consider the Delaunay triangulations¹ of disc centers of P^* and P (see Fig. 4, 5). Notice that in the triangulation of P^* , all triangles are equilateral triangles of side 2. We define the density of a packing in a given triangle to be equal to the proportion of this triangle covered by discs of the packing. The density in any triangle of the triangulation of P^* equals $\frac{\pi}{2\sqrt{3}} = \delta^*$.

It turns out that the density of any triangle in the triangulation of P is less or equal to δ^* , as proven in [CW10]. This allows us to conclude.

This proof is rather simple due to its “locality”: instead of showing that the density of the whole packing P is bounded by δ^* , we show it for each triangle of its triangulation (which is a stronger assertion). Intuitively, the smaller are the units we work on, the more “local” the proof is.

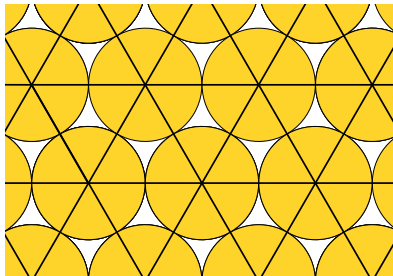


Figure 4: The Delaunay triangulation of the hexagonal packing P^* .

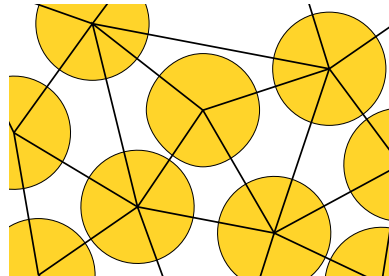


Figure 5: An example of a packing P with its Delaunay triangulation.

Packings of the plane where, as in the hexagonal one, each “hole” is bounded by three pairwise tangent discs are called *triangulated*. More formally,

Definition 1 *A packing is called **triangulated** if the graph formed by connecting the centers of every pair of tangent discs is a triangulation.*

Fejes Tóth in [FT84] called such packings “compact”: since saturated triangulated packings have no “huge holes”, they intuitively look the most compact. Moreover, around each disc, its neighbors form a corona of tangent discs which looks like a locally “optimal” way to pack. For these reasons, triangulated packings appear to be the best candidates to maximize the density on the whole plane.

Notice, that for a fixed n , there exists only a finite number of n -tuples of disc radii (r_1, \dots, r_n) s.t. $1=r_1 > \dots > r_n > 0$ allowing a triangulated packing where all n disc sizes are present [Mes21].

¹See [DO11], especially chapter 23, for the definition and properties of Delaunay triangulations.

1.2.2 2-disc packings

Let us now consider binary packings of the plane. We study the following question: given two discs of radii 1 and $r < 1$, what is the maximal density of a packing by copies of these discs? We can always obtain $\frac{\pi}{2\sqrt{3}}$, the density of the hexagonal packing, by using only one of these discs which gives as a lower bound on the maximal density. Florian in [Flo60] derived an upper bound on the density which is equal to the density in the triangle formed by 2 small and one big pairwise tangent discs. [Fer22] gives tighter lower and upper bounds of maximal density of binary packings of the plane, for all values of $r \in (0, 1)$.

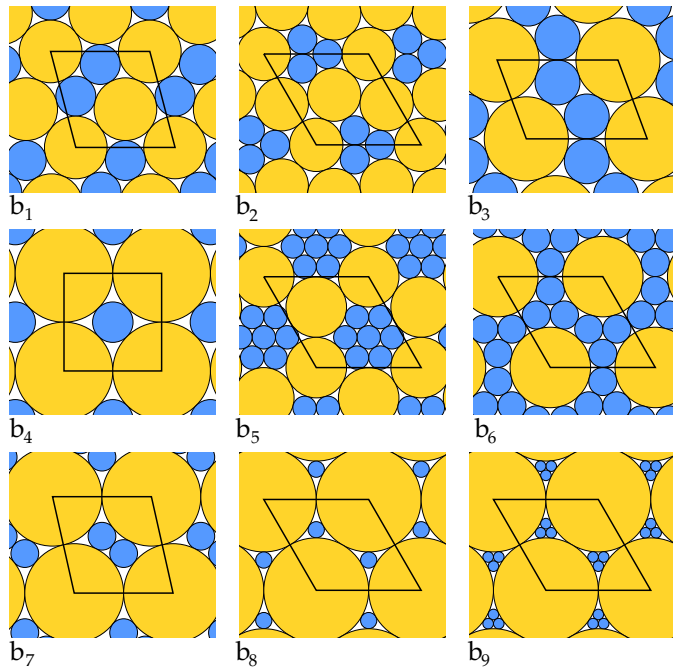


Figure 6: 9 triangulated periodic binary packings maximizing the density among packings with the respective disc sizes.

There are 9 values of r allowing triangulated binary packings where the both disc sizes are present [Ken06]. Such packings are shown in Fig. 6. Each of the depicted packings is *periodic*, i.e. if P is a packing in question, there are two non co-linear vectors u and v , called periods, such that $P + u = P + v = P$. Notice that in this paper, we always consider packings of the whole plane, and since the triangulated packings we show here and below are all periodic, it is enough to represent their fundamental domain

(a parallelogram formed by the period vectors, marked in black in Fig. 6) to see how the whole plane is packed.

Notice that for each of these values of r , there is actually an infinite number of packings having the same density as the one depicted in Fig. 6. First, changing a finite portion of a packings does not affect its density. Moreover, for b_1 , b_3 , and b_7 , there exist non-periodic triangulated packings with a different global structure, having the same density as the ones from Fig. 6 [Ken06]. For the sake of simplicity, we choose to depict the periodic ones.

It turns out that for these 9 radii r , the density is maximized by a triangulated binary packing – namely, the ones shown in Figure 6 [Hep00, Hep03, Ken05, BF22].

This result suggests the following conjecture [CGSY18].

Conjecture 2 (Connelly, 2018) *If a finite set of discs allows a triangulated saturated packing, then the density of packings by these discs is maximized on a triangulated packing.*

This holds for 1-disc packings and 2-disc (*binary*) packings. To study this conjecture, the next step is to verify it for 3-disc (*ternary*) packings which was the main motivation of our work.

2 Result, plan of the paper

Let us turn to the ternary packings. To begin with, we need to find the sizes of discs allowing triangulated ternary packings. This problem was solved in [FHS21]: there are 164 pairs (r, s) featuring triangulated packings with discs of radii $1, r, s$. In this paper, the triplet of discs with radii associated to each of such pairs is called a *case*.

The ternary cases are indexed by positive integers from 1 to 164, like in [FHS21]. To avoid confusion, the binary cases (pairs of disc radii allowing binary triangulated packings) are denoted by b_1, \dots, b_9 which respectively correspond to the cases 1–9 in [BF22].

The Connelly conjecture (Conjecture 2) is applicable only to the cases having triangulated *saturated* packings. This eliminates 15 cases where no triangulated packing is saturated and leaves us with 149 cases.

Our main contribution is a classification of 71 cases formulated in the following theorem:

Theorem 1

- (a) *For the 16 following cases: 53, 54, 55, 56, 66, 76, 77, 79, 93, 108, 115, 116, 118, 129, 131, 146, the density is maximized by a triangulated ternary packing.*
- (b) *For the cases 1–15, the density is maximized by triangulated binary packings. For cases 1–5, it is the triangulated packing of b_8 ; for case 6 — b_4 ; for cases 7–9 — b_7 ; for cases 10–16 — b_9 .*
- (c) *For the 40 following cases: 19, 20, 25, 47, 51, 60, 63, 64, 70, 73, 80, 92, 95, 97, 98, 99, 100, 104, 110, 111, 117, 119, 126, 132, 133, 135, 136, 137, 138, 139, 141, 142, 151, 152, 154, 159, 161, 162, 163, 164, there exists a non-triangulated packing denser than any triangulated one.*

The values of radii corresponding to the cases from Theorem 1 are given in [FHS21]. The triangulated packings maximizing the density for the cases from Th. 1.(a) are depicted in Fig. 7. For Th. 1.(b), the binary triangulated packings which maximize the density are present in Fig. 6 while the ternary triangulated packings are given in Fig. 12. Triangulated ternary packings and non-triangulated binary denser packings for Th. 1.(c) are given in Fig. 13 and in the Appendix A.

All in all, we proved the Connelly conjecture to be false and classified the 149 cases where it was applicable in several groups: 16 cases for which the conjecture holds (Th. 1.(a)), 15 cases where the density is maximized on a triangulated packing using only two discs out of three (Th. 1.(b)), 40 (periodic) counter examples to the initial conjecture (Th. 1.(c)), and the other cases where our proof strategy does not work. Figure 8 represents each case as a point with coordinates $(r, \frac{s}{r})$ and its number from [FHS21]. The color of the point and the number corresponds to the class we assigned to the case.

Section 3 is dedicated to the cases where a ternary triangulated packing is proved to maximize the density. We start by proving Th. 1.(a) (Sections 3.1–3.2). We explain the approach used in the similar proof for binary packings from [BF22] and how we enhance it to make it work in our context. The first improvement was the generalization of the code universal to all the cases (instead of treating them one by one as in [BF22]). The second necessary generalization we made was leaving a bunch of parameters as free variables instead of fixing them arbitrary in the beginning.

Our proof, as quite a few recent results in the domain, like [Hal05, FKS22, Fer22], is based on computer calculations. The main details of the implementation are provided in Section 3.4 (the complete code is given in the

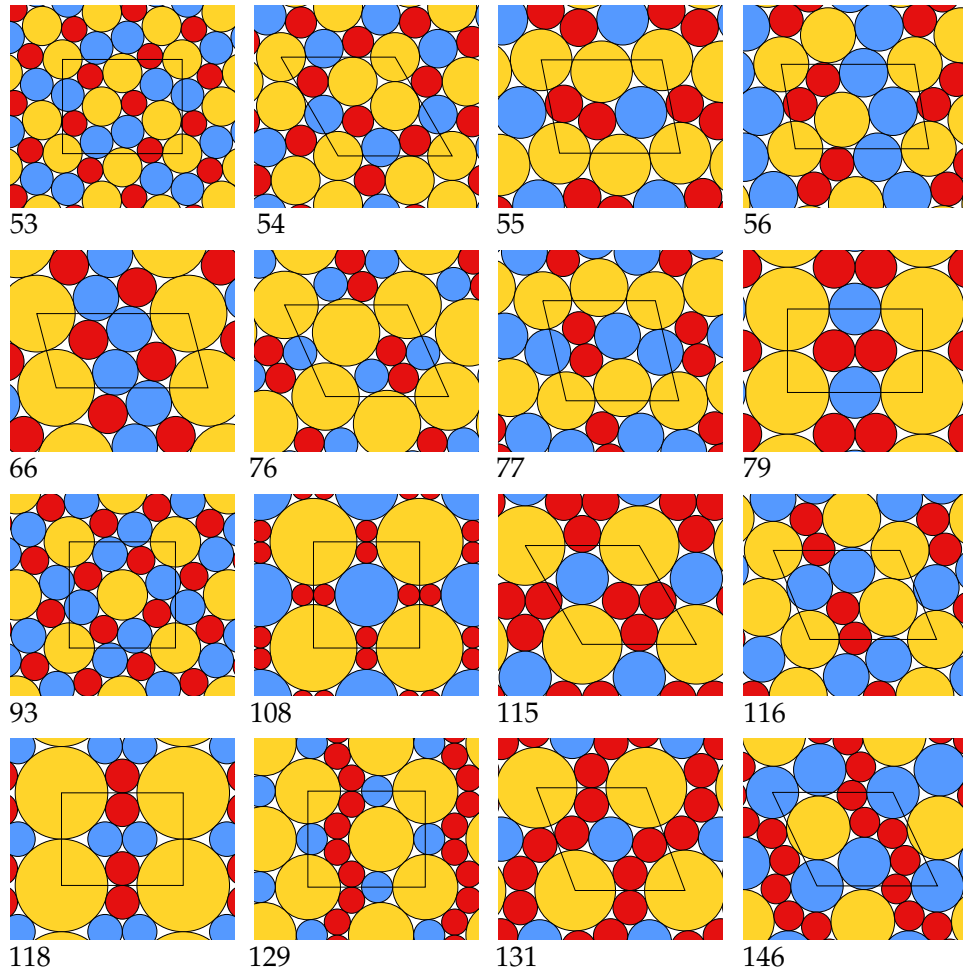


Figure 7: The 16 triangulated ternary packings proved to maximize the density (the numbers correspond to the numbering in [FHS21]).

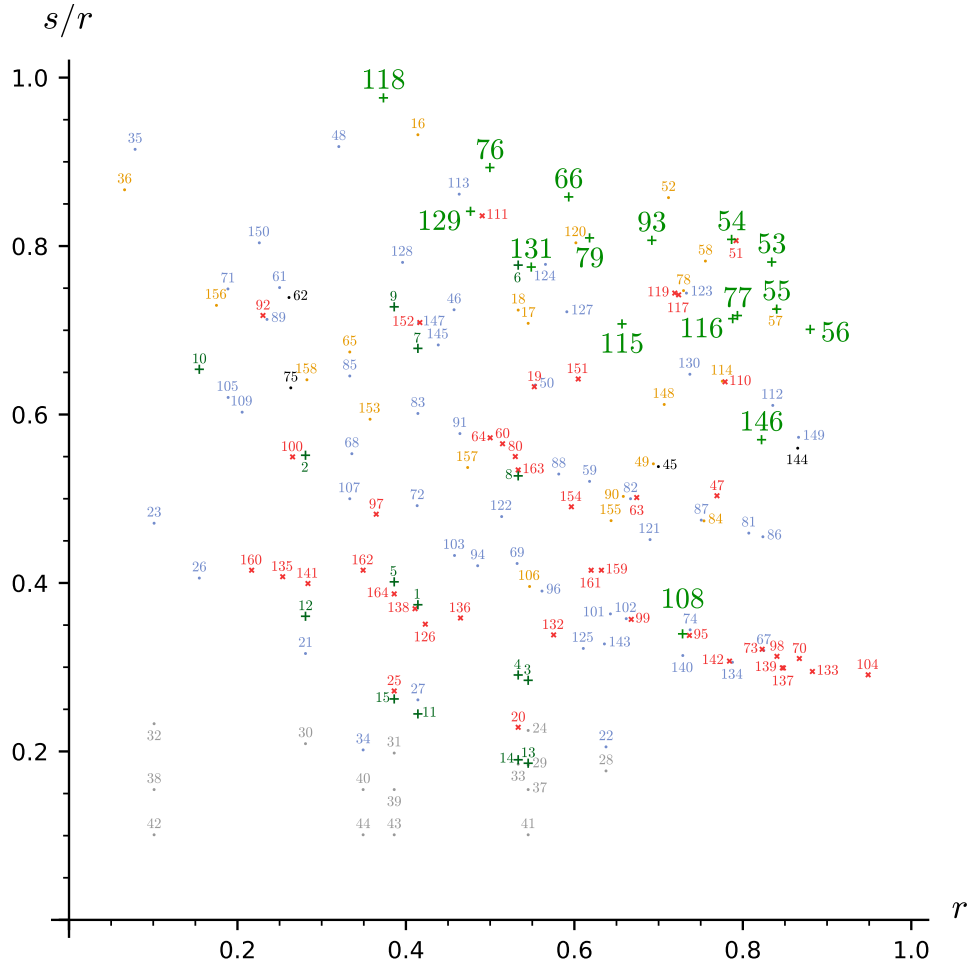


Figure 8: The “map” of the 164 cases with triangulated ternary packings. The cases where no triangulated packing is saturated are marked in grey. The cases with a ternary triangulated packing proved to maximize the density are marked by green + with larger case numbers. The cases where we proved a triangulated binary packing to maximize the density are marked by dark green +. The cases with counter examples are red (x). The cases featuring two coronas (find the details in Section 5.1) are orange. The cases with empty polytopes (see Section 5.2) are blue. The remaining cases are marked in black (Section 5.3).

supplementary materials). We prove Th. 1.(b) in Section 3.5 by adjusting the proof of Th. 1.(a).

Cases from Th. 1.(c) are treated in Section 4. We obtain a counterexample for each of these cases by applying the flip-and-flow method [CG21] on the triangulated binary packings with disc radii ratio close to the radii ratios of pairs of discs of this case.

Section 5 is dedicated to the remaining cases. Section 5.1 presents the 22 cases where one of the discs appears with at least two different neighborhoods. These cases are analogous to the case b5 from Fig. 6 where a small disc is either surrounded by 6 small discs or by two small discs and two big ones. Our proof technique is not sufficient to treat such cases. Handling them requires a less local approach, like it was done in [BF22] for b5.

Section 5.2 treats the 52 cases where we did not find a set of constants satisfying all required inequalities needed in our proof. Even though after several attempts with higher and higher precision, we concluded that the existence of valid constants is quite unlikely, it cannot be rigorously proved for the moment. We thus leave this as an open problem.

Finally, Section 5.3 is dedicated to the 4 cases where the existence of such set of constants is more probable since we could find the parameters satisfying the majority of constraints, but a few of them were still not be satisfied. Whether the density is maximized in these cases is also an open problem.

3 When a triangulated packings is the densest

In this section, we prove the first two parts of Theorem 1.

3.1 Proof strategy of Th. 1.(a)

We follow almost the same steps of the proof as in [BF22] where the same result is proven for binary triangulated packings and in [Fer19] which treats computationally the “simplest” case among the ternary triangulated packings (case 53).

From the theoretical point of view, the transition from binary packings to ternary ones seem to be straightforward. In practice, however, we have much more cases to treat (149 instead of 9) and for each of them, the problem is much more complex due to the high number of local combinatorial configurations in possible packings. This requires a more refined and sensitive choice of parameters than in [BF22].

This section is strongly based on [BF22]: we use the idea of the proof and quite a few intermediate results. Thus, for the sake of simplicity, we preserve the same notations.

Let us describe the theoretical background of the proof which is common for all cases, the only difference being the choice of the parameters described in Section 3.4.

We are given 3 discs of radii $1, r$ and s , $1 > r > s$ and a ternary triangulated packing of the plane by copies of these discs conjectured to maximize the density, let us denote it by P^* . Our aim is to prove that for any other packing P using the same discs, its density $\delta(P)$ does not exceed the density δ^* of P^* .

The main idea common to all the results about the maximal density of triangulated packings was called “cell balancing” by Heppes [Hep03] and it perfectly matches this title. It consists of two steps: first we locally “redistribute” the density among some well-defined cells (triangles of the triangulation in [BF22, Ken05, Hep03] and a mixture of Delaunay simplices and Voronoi cells, both encoded in so-called decomposition stars, in [HF11]) preserving the global density value. Then we prove that the redistributed density of any cell of P never exceeds δ^* .

First, let us define triangulations for packings by several sizes of discs. The *FM-triangulation* of a packing was introduced in [FTM58] (it is a particular case of weighted Delaunay triangulations [DO11]). Some of its useful properties are given in [BF22] (Section 4). The vertices of the FM-triangulation are the disc centers. There is an edge between two disc centers iff there is a point $p \in \mathbb{R}^2$ and a distance $d > 0$ such that p is at distance d from the both discs and at least d from any other disc.

Let \mathcal{T} and \mathcal{T}^* respectively denote the FM-triangulations of P and P^* . The cells we are interested in are triangles of these triangulations. Instead of working with densities, we introduce an additive function E , called *emptiness*, which, for a triangle T in \mathcal{T} , is defined by

$$E(T) := \text{area}(T) \times \delta^* - \text{area}(T \cap P).$$

This function was used in [Ken05] by the name of “excess”. It was inspired by “surplus area” introduced in [Hep03] defined as $\text{area}(T) - \frac{\text{area}(T \cap P)}{\delta^*}$, identical to emptiness up to multiplication by δ^* . A similar but more complex function called “score” is used in the proof of the Kepler conjecture [Lag02].

The emptiness function reflects how “empty” the triangle is compared to δ^* . Indeed, $E(T)$ is positive if the density of T is less than δ^* , negative if

T is denser, and equals zero if $\delta(T) = \delta^*$. We use it rather than the density because of its additivity: the emptiness of a union of two triangles equals the sum of their emptiness values. This property does not hold for the density.

To prove that $\delta \leq \delta^*$, it is enough to show that $\sum_{T \in \mathcal{T}} E(T) \geq 0$ [BF22].

This intuitively means that P is globally more empty and less dense than P^* .

Instead of working directly with the emptiness, we define a so-called potential which plays the role of density redistribution mentioned above. We do it since this function constructed explicitly is easier to manipulate. We will construct a potential U such that for any triangle $T \in \mathcal{T}$, its potential does not exceed its emptiness:

$$E(T) \geq U(T) \tag{2}$$

and the sum of potentials of all triangles in \mathcal{T} is non negative:

$$\sum_{T \in \mathcal{T}} U(T) \geq 0 \tag{3}$$

If, for P^* , there exists U satisfying (2) and (3) for any packing P , then P^* maximizes the density among packings using the same disc radii:

$$(2),(3) \implies \sum_{T \in \mathcal{T}} E(T) \geq 0 \implies \delta^* \geq \delta.$$

The rest of the proof consists in construction of potential U satisfying both (2) and (3) for any packing P .

3.2 How we choose the potential

To construct the potential, we follow the idea first used by Kennedy in [Ken05] who introduced the “localizing potential” being inspired by a statistical mechanics notion of “m-potentials”. We define the total potential of a triangle as a sum of potentials of “smaller” units. It will consist of three *vertex potentials* \dot{U} defined in the next section and three *edge potentials* \bar{U} (Section 3.2.2). Emptiness redistribution takes place through vertex and edge potentials: the sum of vertex potentials around each vertex in the triangulation will be non negative as well as the sum of two edge potentials of triangles sharing this edge. These two conditions guarantee us the “global” inequality (3).

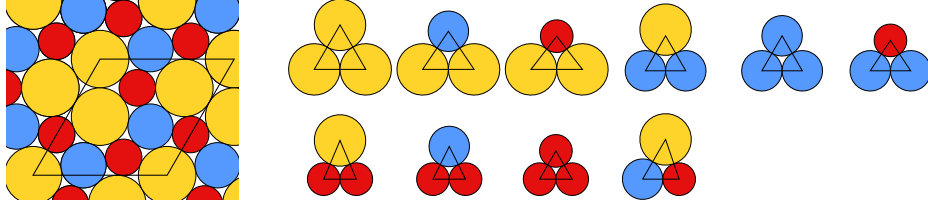


Figure 9: Case 54, its triangulated packing (left) and its 10 tight triangles (right).

All in all, the next four sections follow Sections 5.1-5.2, 6 and 7 of [BF22]: we are constructing the potential in a way that the global inequality (3) is satisfied, at the same time trying to minimize the potential of each triangle. The last step is to verify for any triangle that the local inequality (2) is also satisfied, this part is discussed in Section 3.3.

3.2.1 Vertex potentials

We denote the first part of the potential by \dot{U} , it is composed of three vertex potentials: if A , B , and C are the vertices of triangle T in the FM-triangulation \mathcal{T} of packing P ,

$$\dot{U}(T) := \dot{U}_A(T) + \dot{U}_B(T) + \dot{U}_C(T).$$

Notice that we use the same notations as in [BF22] except that we add a dot above the vertex potentials and a bar above the edge potentials to differentiate them more easily.

We seek to choose the vertex potentials in a way to satisfy the following inequality around any vertex $v \in \mathcal{T}$:

$$\sum_{T \in \mathcal{T} | v \in T} \dot{U}_v(T) \geq 0. \quad (\bullet)$$

This inequality implies global inequality (3) for vertex potentials.

A triangle is called *tight* if it is formed by three pairwise tangent discs. It is known that the properties of the FM-triangulation imply that all triangles of a triangulated packing are tight. For each set of three distinct disc radii, there are 10 tight triangles, one for each triplet of discs (see Figure 9). Let E_{xyz} denote the emptiness of the tight triangle formed by discs of radii x, y, z . We denote by V_{xyz} the vertex potential of this triangle in the vertex corresponding to the y -disc. Since we set $V_{xyz} = V_{zyx}$, there are 18 of them.

Inequalities (2) and (3), applied to \mathcal{T}^* , imply the following constraints on the vertex potentials of tight triangles appearing in \mathcal{T}^* . For each tight

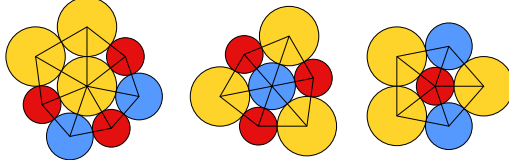


Figure 10: Three coronas of packing 54.

triangle T in \mathcal{T}^* , $\dot{U}(T) = E(T)$ and for each vertex v in \mathcal{T}^* ,

$$\sum_{T \in \mathcal{T}^* | v \in T} \dot{U}_v(T) = 0. \quad (4)$$

The latest means that the sum of vertex potentials in v of all triangles surrounding it (the set of these triangles is called the *corona* of v) equals zero. Let us illustrate it with the case 54 whose triangulated packing is given in Fig. 9. There are only three types of tight triangles present in this packing, so the first class of constraints produces the following equations:

$$3V_{111} = E_{111}, \quad V_{1s1} + 2V_{11s} = E_{1s1}, \quad V_{1rs} + V_{rs1} + V_{s1r} = E_{1rs}.$$

The equations for the three coronas given in Fig. 10 are respectively:

$$V_{111} + 2V_{11s} + 4V_{r1s} = 0, \quad 6V_{1rs} = 0, \quad V_{1s1} + 4V_{1sr} = 0.$$

We thus have 18 variables and 6 equations with only 5 of them being independent due to periodicity of the packing: since the sum of the emptiness of tight triangles of the fundamental domain of the packing equals zero, there is a linear combination of tight triangle potentials equal to zero.

We also set the potentials of all other tight triangles equal to their emptiness. In our example, this gives us 7 more equations that are still independent and leaves us with 6 free variables.

Until now we followed the strategy used in [BF22] which does not work for the cases proved here, except the case 53 proved earlier in [Fer19]. The problem is that in [BF22, Fer19], the free variables mentioned above are all directly set to zero to simplify further computations. The first generalization we made was to keep these 6 variables as free variables and fix them later, in order to satisfy all inequalities (2) around the vertices. The 6 tight vertex potentials left free are the vertex potentials of the isosceles (but not equilateral) tight triangles in the vertex adjacent to the two equal edges. More formally, the free variables are the following:

$$\{V_{xyx} \mid x, y \in \{1, r, s\}, x \neq y\}.$$

These variables are always independent and independent of the equations.

The next step is to choose the vertex potentials of all the other (non tight) triangles in a way that inequalities (2) and (3) hold.

As in Section 5.2 of [BF22], we define them as follows:

$$\dot{U}_v(T) := V_{xyz} + m_y |\hat{v} - \widehat{xyz}|,$$

where x, y, z are the disc sizes of T , v is the vertex corresponding to the y -disc, \hat{v} is the angle of T in v , \widehat{xyz} is the angle in the vertex of the y -disc in the tight triangle with discs of radii x, y, z , and m_y is a constant defined below. The difference between the vertex potential of T and the vertex potential of the tight triangle with the same discs is proportional to their angle difference, or “how different triangle T is from the tight one”. The constants m_1, m_r, m_s reflecting the “importance” of this angle deviation in vertex potentials should be chosen carefully, which is explained below.

Given a triangle T with discs of radii x, y, z in \mathcal{T} , let T^* denote the tight triangle formed by the same discs.

Our aim now is to choose the tight vertex potentials and m_1, m_r, m_s in a way that inequality (\bullet) holds around each vertex. This is the case if, for each vertex v with disc of radius q in \mathcal{T} , the following inequality is satisfied:

$$m_q \geq \frac{-\sum_{j=1}^k \dot{U}(T_j^*)}{\left| 2\pi - \sum_{j=1}^k \hat{v}(T_j^*) \right|}, \quad (5)$$

where T_1, \dots, T_k is the corona of v in \mathcal{T} .

The proof is identical to the one for binary packings given in [BF22]. Notice that the only case where the denominator equals zero is when T_1^*, \dots, T_k^* form a corona in the triangulated packing. The sum of vertex potentials of triangles in such corona equals zero by (4).

We thus have to choose the tight vertex potentials and m_1, m_r, m_s satisfying these inequalities. As explained in the proof of Proposition 3 of [BF22], it is enough to perform an exhaustive search on a finite number of configurations to assure this inequality. It thus can be done by a computer.

The 6 values of potentials V_{xyz} of tight triangles which were left as free variables, as well as m_1, m_r, m_s , are chosen to satisfy inequality (5). The solutions of this inequality (a subset of \mathbb{R}^9) are the appropriate combinations of values of potentials and m_1, m_r, m_s . The details of computer implementation of this part and how we choose the precise values are described in Section 3.4.2.

Furthermore, using Proposition 4 from Section 6 of [BF22], we can cap each vertex potential with a constant value depending only on the disc type of the vertex. The proof of this proposition roughly consists in showing that for any vertex, as soon as the vertex potential of a triangle in its corona exceeds a certain value, the remaining vertex potentials will never be “too negative” which implies inequality (\bullet) in this vertex.

This allows us to diminish vertex potential while still satisfying its non negativity around each vertex (\bullet) . It was not needed in [Fer19] for case 53 but turns out to be necessary for all the other cases we consider. Thus, the vertex potential of triangle T in vertex v corresponding to a q -disc will be rewritten as $Z(\dot{U}_v(T)) = \min(\dot{U}_v(T), Z_q)$ where

$$Z_q := 2\pi \left| \min_{T_{xqz} \in \mathcal{T}} \frac{V_{xqz}}{xqz} \right|.$$

3.2.2 Edge potentials

As in Section 7 of [BF22], in order to keep the potential lower than the emptiness in all triangles (to satisfy inequality (2)), we introduce its second part, \bar{U} , called the edge potential. We can now write down the total potential $U(T)$ of a triangle T :

$$U(T) := Z(\dot{U}(T)) + \bar{U}(T).$$

We need \bar{U} to compensate the vertex potential of “stretched” triangles: those where one angle is too large. Such triangles feature high vertex potential and low emptiness. The edge potential of a triangle is equal to the sum of edge potentials corresponding to its three edges: if e, d, f are the edges of triangle T , $\bar{U}(T) := \bar{U}_e(T) + \dot{U}_d(T) + \dot{U}_f(T)$.

We define the edge potential of T in e as follows:

$$\bar{U}_e(T) := \begin{cases} q_{xy}d_e & \text{if } |e| > l_{xy} \\ 0 & \text{otherwise} \end{cases}$$

where x, y are the radii of the discs with centers in the endpoints of edge e and d_e is the signed distance from the center X of the circumscribed circle of T to e (d_e is positive iff X and T are at the same side with respect to e). The choice of the constants q_{xy}, l_{xy} is explained below.

With this definition, the sum of edge potentials of two triangles sharing this edge is always non negative. This is shown in [BF22] (Section 7, Proposition 3). Thus, adding the edge potential keeps the global inequality (3)

valid. Meanwhile, it affects the local distribution of potentials among neighbour triangles approaching us to our aim which is to satisfy $E(T) \geq U(T)$ in all triangles.

We pick the pairs of constants q_{xy} and l_{xy} (there are 6 of them, one for each pair (x, y) of disc radii) in order to compensate high vertex potential of stretched triangles. To find constants allowing to do this, we compute the vertex potential and the emptiness of the most “dangerous” triangles: those with two pairs of tangent discs (see an example in Figure 11). We represent them as curves in function of the length of the only “flexible” edge.

To choose q_{xy} and l_{xy} for given (x, y) , we consider three triplets of discs radii: $x1y, xry, xsy$ and for all of them we trace the curves as ones shown in Figure 11. The aim of edge potential is not to let the capped vertex potential $Z(\dot{U}_v(T))$ (**dashed red line**) exceed the emptiness $E(T)$ (**dark blue line**). In all the cases considered here, the capped vertex potential and the emptiness have at most one intersection except the leftmost point corresponding to the tight triangle (the neighborhood of this point is a special case treated in detail in Section 3.3.1). This intersection is the side length such that stretching the triangle even more causes vertex potential to be greater than emptiness.

Let l_{xqy}^* be the side length where this intersection occurs for a triangle formed by discs with radii x, q, y . Notice that d_e is a decreasing monotonous function on the side length $|e|$. If $d_{l_{xqy}^*} < 0$ (which is the case for all the proved cases), then it is enough to set l_{xy} equal to at most $l_{xqy}^* - \alpha$ with a small enough α (we used $\alpha = 10^{-5}$). We thus set

$$l_{xy} := \min_{q=1,r,s} l_{xqy}^* - \alpha.$$

As an illustration, when choosing q_{ss} and l_{ss} for case 54 (see Fig. 11), the triangle with discs of radii s, s, s has the leftmost intersection of $E(T)$ and $Z(\dot{U}_v(T))$ (* on the first graph). This means, $l_{ss} = l_{sss}^* - \alpha$.

Then we choose the coefficient q_{xy} in a way that $Z(\dot{U}_v(T)) + d_e q_{xy}$ stays below E starting from $l_{xqy}^* - \alpha$ for all $q = 1, r, s$ (which is always possible since d_e is negative on this segment).

These choices guarantee the total potential $U(T)$ (**bold red line** in Fig. 11) to be below the emptiness all the way from tight to stretched triangles.

3.3 Verifying local inequality (2)

In Section 3.2, we constructed the potential in a way that the global inequality (3) is satisfied. We should now prove that for any triangle T , (2)

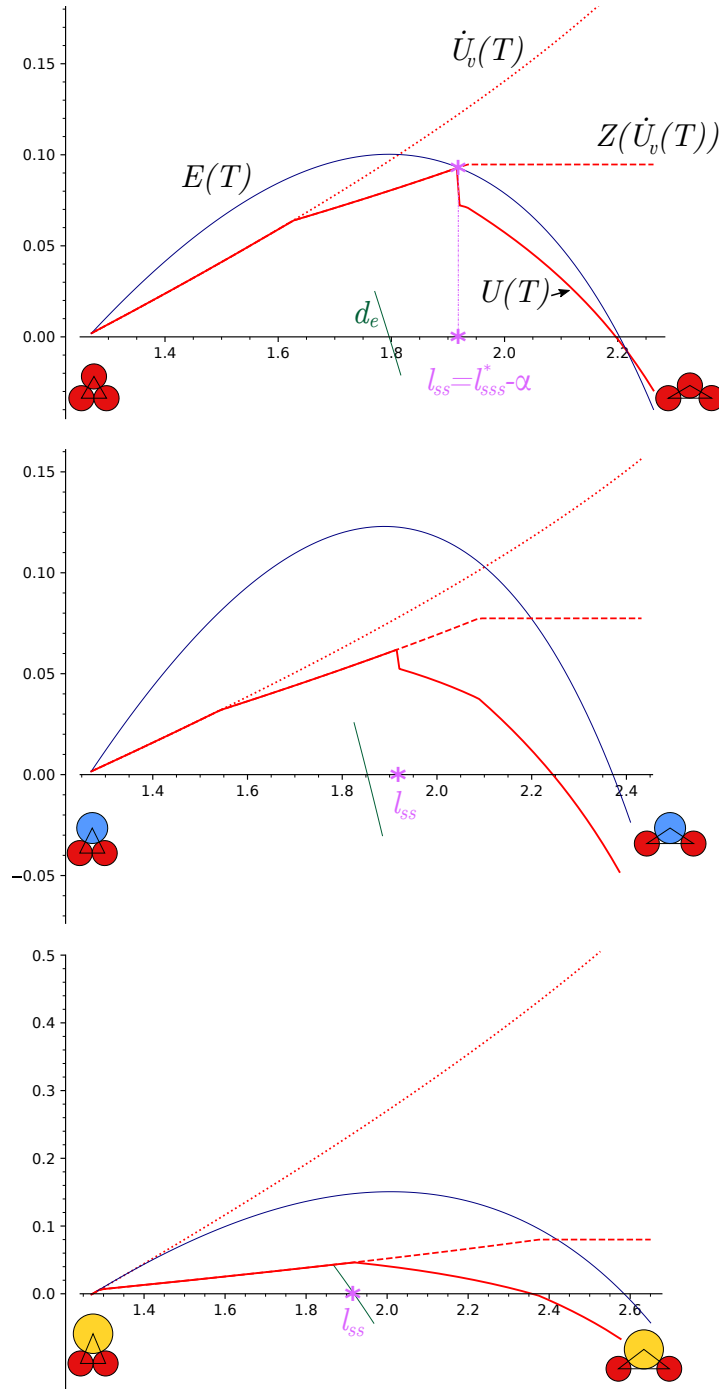


Figure 11: Case 54, triangles with discs sss , srs , sls : behavior of the emptiness (in dark blue) and the potential while stretching an edge. Initial vertex potential $\dot{U}_v(T)$ is marked by the dotted red line, capped vertex $Z(\dot{U}_v(T))$ potential is the dashed red line, the total potential $U(T)$ is the bold red line. The dark green segment designates d_e around the moment it becomes negative, and the pink asterisk $*$ indicates the value of l_{ss} .

holds: $E(T) \geq U(T)$. This part widely uses computer calculations: we execute them in SageMath ². We first treat the triangles that are close to the tight ones, so-called *epsilon-tight triangles*, in Section 3.3.1. For all the other triangles, (2) is verified in Section 3.3.2.

3.3.1 Epsilon-tight triangles

As in Section 8 of [BF22], the definition of the vertex potential allows us to directly show that it does not exceed the emptiness in the triangles “close enough” to the tight ones. We do it by comparing the differentials of the two functions. We are interested in this case since tight triangles are the limiting point where the emptiness is equal to the potential.

Let \mathcal{T}_ϵ denote the set of *epsilon-tight* triangles, those where each pair of discs is at distance at most ϵ . We can bound the variation ΔE of emptiness on \mathcal{T}_ϵ :

$$\Delta E \geq \sum_{i=1,2,3} \min_{\mathcal{T}_\epsilon} \frac{\partial E}{\partial x_i} \Delta x_i,$$

where x_1, x_2, x_3 are the lengths of the sides.

We consider only the values of ϵ that are strictly smaller than the l_{xy} -constants so that edge potentials do not play a role in this case: since the smallest l_{xy} is greater than ϵ , we can find the lower bound of the variation ΔU of potential:

$$\Delta U \leq \sum_{i=1,2,3} \max_{\mathcal{T}_\epsilon} \frac{\partial U}{\partial x_i} \Delta x_i.$$

As we have set the potential equal to the emptiness on tight triangles, choosing ϵ such that for $i = 1, 2, 3$,

$$\min_{\mathcal{T}_\epsilon} \frac{\partial E}{\partial x_i} \Delta x_i \geq \max_{\mathcal{T}_\epsilon} \frac{\partial U}{\partial x_i} \Delta x_i \tag{6}$$

guarantees us that the local inequality (2) is satisfied by all triangles in \mathcal{T}_ϵ .

To find the greatest value of ϵ satisfying this inequality, we use a dichotomic search, aiming to maximize ϵ (indeed, maximizing the set \mathcal{T}_ϵ we minimize the set of the remaining triangles that should be treated afterwards). At each step of the binary search, we compute both values in interval arithmetic (explained in the next section and Section 3.4.1) and if the

²<https://www.sagemath.org/>

intervals of these values do not intersect and satisfy inequality (6), the given ϵ is valid.

3.3.2 Other triangles

The final step is to verify the local inequality (2) on the set of non epsilon-tight triangles that could appear in a triangulation of a packing. Thanks to the properties of FM-triangulations of saturated packings, this set is compact. Indeed, the length of the edge connecting centers of discs of radii x and y in a triangle is at least $x+y$ and at most $x+y+2s$. The *support circle* of a triangle in a packing is the circle tangent to the three discs with centers in the vertices of the triangle. Thanks to FM-triangulation properties, the support circle never intersects other discs of the triangulation. The upper bound on the side length comes from the fact that the radius of the *support circle* is at most s (otherwise the packing would not be saturated). Thus, if the centers of the two discs are respectively X and Y and the support circle center is O , applying the triangle inequality to XOY , we get $|XY| \leq x + y + 2s$.

Working with intervals rather than precise values allows us to decompose a compact continuum set of cases into a finite one. Given a triplet of disc radii, each side of each triangle with these 3 discs in vertices is bounded. Therefore, to prove inequality $E(T) \geq U(T)$ for all triangles with given disc radii, it is enough to show it for the triangle with sides represented by intervals depending on these radii. More precisely, we should verify the following inequality:

$$E(\overline{T}_{xyz}) \geq U(\overline{T}_{xyz}),$$

where \overline{T}_{xyz} is a triangle with discs of radii x, y, z and sides represented by intervals $[y+z, y+z+2s], [x+z, x+z+2s], [x+y, x+y+2s]$. If it holds (the returned value is **True**), then the inequality holds for all possible triangles with discs x, y, z . If the returned value is **False**, this means either that the inequality is false or that the intervals in question intersect (and thus are incomparable). In this case, we subdivide initial intervals augmenting precision. Section 3.4.1 describes in detail how it is done in practice, using interval arithmetic tools of SageMath.

3.4 Computer implementation

As many proofs of the domain, notably the proof of the Kepler Conjecture [Hal05], the proofs of the maximal density for triangulated packings, like ours and those from [BF22, Fer19, Ken05], essentially rely on computer

calculations. In this section, we discuss the details of computer implementation.

The treatment of each case consists of two steps. We first choose all the values necessary to define the potential: tight vertex potentials V_{xqy} , constants m_q and capping values Z_q from Section 3.2.1, the value of ϵ (Section 3.3.1), and the constants l_{xy}, q_{xy} of the edge potentials (Section 3.2.2). We choose them in a way to satisfy the “global” inequality (3). The second step is to verify the “local” inequality (2) on all possible triangles explained in Section 3.3.2.

3.4.1 Interval arithmetic

We use interval arithmetic in two completely different contexts: to work with real numbers non representable in computer memory and to verify inequalities on uncountable but compact sets of values. More precisely, we use intervals to store the values of radii of discs which are algebraic numbers obtained as roots of polynomials in [FHS21] as well as the value of π . The other situation where we use intervals is to verify the local inequalities on a compact continuum set of triangles in Section 3.3.2.

In interval arithmetic, each value is represented by an interval containing this value and whose endpoints are exact values finitely representable in computer memory (floating-point numbers). Performing functions in interval arithmetic preserves both properties. More precisely, if x_1, \dots, x_n are intervals, and f is an n -ary function, the interval $f(x_1, \dots, x_n)$ must contain $f(y_1, \dots, y_n)$ for all $(y_1, \dots, y_n) \in x_1 \times \dots \times x_n$ and its endpoints are floating-point numbers.

To verify an inequality on two intervals $x_1 < x_2$, it is enough to compare the right endpoint of x_1 and the left endpoint of x_2 . The returned value is `True` only if each pair of values from these intervals satisfy the inequality. However, if the result is `False`, that does not mean that the inequality is false on the numbers represented by x_1 and x_2 , it might also mean that these intervals overlap.

We worked with interval arithmetic implemented in SageMath [Dev20], called Arbitrary Precision Real Intervals³. The intervals endpoints are floating-point numbers, the precision we use in the majority of cases is the default precision of the library where the mantissa encoding has 53 bits.

³https://doc.sagemath.org/html/en/reference/rings_numerical/sage/rings/real_mpfi.html

3.4.2 Polyhedra

In Section 3.2.1, we choose the values of vertex potentials in tight triangles and constants m_1, m_r, m_s in a way to satisfy all the necessary constraints. These constraints together define a subset of \mathbb{R}^9 (where the variables are 6 tight vertex potentials $V_{1r1}, V_{1s1}, V_{r1r}, V_{rsr}, V_{s1s}, V_{srs}$ and 3 constants m_1, m_r, m_s). We use the Polyhedra module⁴ of SageMath to work with them (it allows us to store the solutions of a system of linear inequalities as a convex polyhedron).

Even more constraints are added in Section 3.3.1, since there should exist a positive value of ϵ satisfying the inequalities (6). To guarantee that, we verify if inequality (6) holds for $\epsilon = 0$, in other words, we make sure that this inequality holds for some non-negative ϵ . We do it in SageMath: to compute both parts of the inequality, we use interval arithmetic and calculations of derivatives. The obtained inequalities are intersected with the polyhedron calculated above. For all the cases considered in this section, this intersection is not empty (the cases where it was empty are discussed in Section 5.2). Then we find the maximal value of $\epsilon > 0$ allowing the intersection not to be empty and this permits us to fix ϵ .

For all the cases we treat in this section, these constraints together define a compact polyhedron in \mathbb{R}^9 (where the variables are the 6 tight vertex potentials and m_1, m_r, m_s).

After we get a polyhedron of valid values, we are free to choose a point inside to fix them. Our aim at that step is to minimize potentials of all triangles in order to satisfy (2). We thus find the three vertices of the polyhedron minimizing m_1, m_r and m_s respectively, compute a linear combination of them (the weights that worked well in practice were respectively 1,1 and 4), and take a point between this one and the center of the polyhedron in order to avoid the approximations problems on the border which are discussed in the next paragraph. Our method to choose the point described above is a heuristic.

Implementing construction of polyhedra, we encounter the following problem: the Polyhedra class does not allow coefficients of constraints to be intervals, while some of the coefficients of our inequalities are stored as such due to their dependency of π and disc radii. Polyhedra do not support intervals as a base ring for a good reason: solutions of a system of linear inequalities with interval coefficients might not form a convex polyhedron. We choose to replace the intervals with their centers and work with

⁴https://doc.sagemath.org/html/en/reference/discrete_geometry/sage/geometry/polyhedron/constructor.html

an approximation of the actual set of valid values for tight potentials and m_1, m_r, m_s . Our polyhedron is stored in a field of rational values, since this field is computationally quite efficient.

That means, after choosing a point inside this approximated polyhedra, we can not know if this point actually satisfies all the constraints. To make sure it does, we then rigorously verify that all the inequalities with interval coefficients hold in this point.

3.5 Proof of Th. 1.(b)

Cases 1-18 are special: they are called *large separated* in [FHS21] since they do not contain pairs of adjacent medium and small discs (see Fig. 12 for the first 15). For each of these cases, in addition to ternary triangulated packings, there are other triangulated packings using only two discs out of three. It happens because the radii of small and medium discs coincide with the radii of small discs of two cases among b_1 - b_9 . It is thus possible to assemble packings having the same density as the binary packings of mentioned cases using only two of three discs. It turns out that in all these cases, the density of one of the mentioned binary packings exceeds the density of the ternary one. That means, for each of cases 1-18, the densest packing among the triangulated ones is a binary packing corresponding to a case from b_1 - b_9 (Fig. 6).

Indeed, each of these ternary packings is formed as a “combination” of two binary packings one of which is denser than the other. Thus, the densest of the binary packings will also be denser than its combination with a less dense packing.

We were able to show that the denser triangulated binary packing maximizes the density among all packings (not only triangulated ones) for the cases from 1 to 15 (Fig. 12). The proof is almost the same as in Section 3.

Let i be the case number and P_3 denote its triangulated ternary packing. Let P_2^* denote the densest triangulated binary packing using two discs of case i and let P_2 denote the less dense triangulated binary packing using two discs of case i . We already know that P_2^* is denser than the two others, $\delta(P_2^*) > \delta(P_3) > \delta(P_2)$. Our aim is to show that P_2^* maximizes the density among all packings by the discs of case i .

The only difference with the strategy used for other cases concerns vertex potentials from Section 3.2.1. Since P_2^* uses only two discs out of three, it features only 2 coronas instead of 3. Thus, these 2 coronas together with the 10 equations for tight triangles, give us at most 11 independent equations instead of 12.

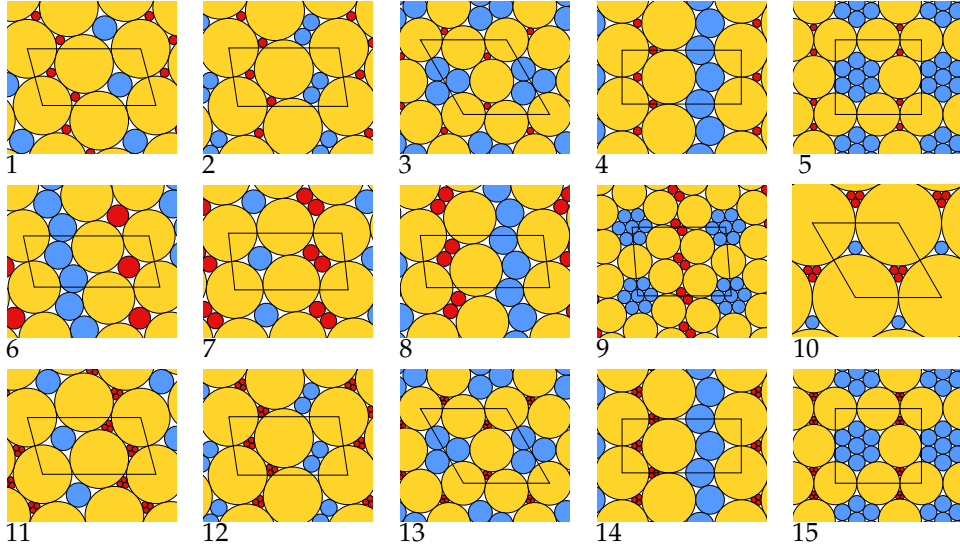


Figure 12: Triangulated ternary packings for cases 1-15, where a triangulated binary packing maximizes the density. For cases 1-5, it is the triangulated packing of b_8 ; for case 6 — b_4 ; for cases 7-9 — b_7 ; for cases 10-16 — b_9 .

We now need to choose 7 free variables instead of 6. We can pick 6 tight potentials of isosceles triangles as before. There remains to choose the last free variable. Vertex potentials of equilateral tight triangles can not be picked because of the equations of type $V_{xxx} = E_{xxx}$: they are already fixed. The remaining vertex potentials of isosceles triangles (V_{xxy} , $x \neq y$) can not be used since they are dependent of the first 6 free variables and the equations $2V_{xxy} + V_{xyx} = E_{xyx}$. The only candidates thus are V_{1rs} , V_{1sr} , V_{r1s} ; we add one of them.

For cases 16, 17, and 18, the densest binary packing is b_5 which features two different coronas around the small disc, so our method is not applicable to them as discussed in Section 5.1.

To summarize, for cases 1-18, among triangulated packings, the density is maximized by a binary packing, not a ternary one as in the Connelly conjecture. However, whether this packing maximizes the density among all packings is still an open question for cases 16, 17 and 18.

4 Counter-examples: proof of Th. 1.(c)

Starting to work on the density of ternary saturated triangulated packings, we believed the Connelly conjecture to hold, i.e. that for all of the 149 cases, a triangulated packing would maximize the density. Realization that our proof strategy failed for many of them made us suspect the conjecture to be false. Knowing that the density of binary triangulated packings (all of them are given in Figure 6) often exceeds the density of ternary triangulated packings in question gave us an idea to use them in order to find counter examples.

The first result we obtained was for case 110 [FP21]. After generalization, we ended up with 40 counter examples (19, 20, 25, 47, 51, 60, 63, 64, 70, 73, 80, 92, 95, 97, 98, 99, 100, 104, 110, 111, 117, 119, 126, 132, 133, 135, 136, 137, 138, 139, 141, 142, 151, 152, 154, 159, 161, 162, 163, 164). They are all non triangulated packings using only two discs out of three which have greater densities than triangulated packings using all three discs. We obtained each of them deforming a triangulated binary packing with discs whose size ratio is close to the one of a pair of discs in the triplet associated to the case. Tiny deformations do not dramatically lower the density and these packings are dense enough to outplay the ternary triangulated ones.

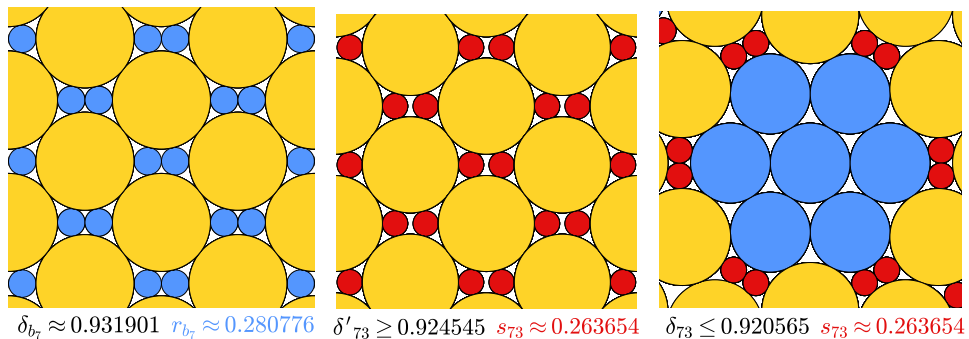


Figure 13: Left: a triangulated binary packing of case b_7 . Middle: a deformation where the small discs are replaced with the small discs of case 73. Right: a triangulated periodic packing of case 73, its fundamental domain and description are given in [FHS21].

Let us explain our method on an example. Recall that the pairs of discs allowing binary triangulated packings are denoted by b_1, \dots, b_9 while the triplets with ternary triangulated packings are indexed by positive integers from 1 to 164. Let us consider case 73, its triangulated ternary packing is given in Figure 13, on the right. Notice that the radius of the small disc

($s_{73} \approx 0.263$) of case 73 is close to the radius of the small disc ($r_{b_7} \approx 0.281$) of case b_7 . Let us deform the triangulated binary packing of b_7 (Figure 13, on the left) replacing the small disc of b_7 by the small disc from 73. We choose a deformation which breaks as few contacts between discs as possible: the one given in the center of Figure 13. Observe that the only broken contact is between the two small discs: they are not tangent anymore. The density of this new non-triangulated packing $\delta' \approx 0.9245$ is higher than the density of the triangulated packing 73 $\delta_{73} \approx 0.9206$ (Figure 13, on the right).

This method is called flip-and-flow [CG21]. The 40 counter examples were found by computer search. First, for each case b_i , we find the set of pairs of radii from the cases 1-164 with radii ratio “close enough” (we choose the distance heuristically) to the ratio of the discs of b_i . Then we deform the triangulated packing of b_i to obtain packings with the found disc ratios. Our way to deform packings was chosen in order to minimize the number of broken contacts between discs since intuitively it is the best way to keep the density high. Finally, the densities of 40 packings obtained by our method were higher than the densities of the respective ternary triangulated packings which leaves us with the counter examples given in Appendix A.

Our method is not universal: there might be other deformations for certain cases to obtain even higher density and even more counter examples. Besides that, there might be other cases with ternary counter examples (notably, among the cases discussed in Sections 5.2).

5 Other cases

5.1 2 coronas

Among the necessary conditions on vertex potentials in tight triangles given in Section 3.2.1, we saw that the sum of potentials in the corona around any vertex of triangulated packing T^* must be equal to zero. In all the proved cases, each disc has only one possible corona in T^* . It is not always the case, more precisely, among the cases where T^* is saturated, and for which we did not find counter examples, there are 22 cases where one of the discs appears with at least two different coronas in T^* : 16, 17, 18, 36, 49, 52, 57, 58, 65, 78, 84, 90, 106, 114, 120, 148, 153, 155, 156, 157, 158, 160. Each of these cases features a supplementary corona consisting of 6 discs of the same size as the central one. We thus have to add a supplementary condition $6V_{xxx} = 0$, where x is the radius of the disc with two coronas. This however contradicts the condition $3V_{xxx} = E_{xxx}$ in all of these cases. Our density redistribution would need to be less local to solve this problem. In the context of binary

triangulated packings, such a case (b_5 , see Figure 6) is treated in detail in Section 5.3 of [BF22].

5.2 Empty polyhedra

In Section 3.4.2, we construct a polyhedron in \mathbb{R}^9 aiming to contain all valid values of tight vertex potentials and m_1, m_r, m_s . In this Section, we talk about the 52 cases where the polyhedron obtained by our computations is empty: 21, 22, 23, 26, 27, 34, 35, 46, 48, 50, 59, 61, 67, 68, 69, 71, 72, 74, 81, 82, 83, 85, 86, 87, 88, 89, 91, 94, 96, 101, 102, 103, 105, 107, 109, 112, 113, 121, 122, 123, 124, 125, 127, 128, 130, 134, 140, 143, 145, 147, 149, 150.

The polyhedron formed by the inequalities from Section 3.2.1) and inequality (6) for $\epsilon = 0$, represents the values satisfying (\bullet) featuring a non-negative valid ϵ . These constraints are necessary for our proof to be correct. If this polyhedron is empty there are no valid values of tight potentials and m_1, m_r, m_s and thus our strategy of proof is not applicable.

Nevertheless, our computations are limited by computer memory which can represent only certain values. Normally, we avoid this problem by using interval arithmetic (Section 3.4.1). However, we can not apply this solution with polyhedra. First, as mentioned in Section 3.4.2, in SageMath, the polyhedra module does not support the interval field as a base ring. Implementing another way to represent “interval polyhedra” would be unreasonable due to memory and time constraints of calculations: the polyhedra are constructed from thousands of inequalities, and performing computations in interval field significantly increases time and memory costs. Instead, we use the ring of rationals to store the inequalities coefficients. Therefore, the polyhedron we work with is an approximation of the actual polyhedron and may not contain all the valid sets of values.

Yet, we believe that the polyhedra in question are probably actually empty in these cases, so the precision issues are not the principal obstacle. All in all, some of the cases from this section might actually maximize the density but we would need an essentially different approach to be able to prove it. Looking forward, further attempts to treat these cases would likely need to use a less local density distribution.

5.3 The 4 mysterious cases

In the four remaining cases (45, 62, 75, and 144) the polyhedron from Section 3.4.2 is not empty, like for the cases from the previous section. Nevertheless, we could not find a point in it to guarantee the local inequality (2)

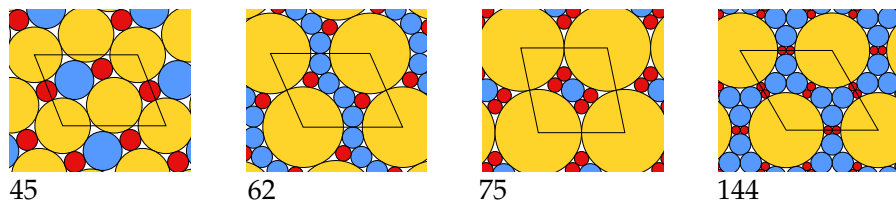


Figure 14: Triangulated ternary packings of the four *mysterious* cases.

in all triangles: the problematic triangles are always those close to one of the tight ones. Minimizing m_q and the tight potentials is an obvious strategy to minimize the potentials and eventually satisfy (2) but the capping constants Z_q also dramatically affect potentials.

Trying to find appropriate values of V_{xyz} , m_q and z_q , we represented them with all the constraints coming from (3) as a linear optimization problem. This allowed us to encode problematic triangles violating (2) as constraints and add them to the system, one by one, each time one appears during local verification (Section 3.3.2), in hope to finally “converge” to a solution which would satisfy (2) on all triangles. However, this method failed: no solutions were found.

The fact that we could not choose a set of appropriate constants in these cases does not prove that they do not exist (due to the approximation issues already discussed in the previous section as well as the new ones coming from encoding our constraints into a rational linear problem). We, however, believe that these cases, as well as those from the previous section, just can not be treated by our proof methods. They probably require a less local emptiness redistribution than the one we use.

References

- [BF22] N. Bedaride and T. Fernique. Density of Binary Disc Packings: The Nine Compact Packings. *Discrete and Computational Geometry*, 67:1–24, 2022.
- [CG21] R. Connelly and S. J. Gortler. Packing Disks by Flipping and Flowing. *Discret. Comput. Geom.*, 66:1262–1285, 2021.
- [CGSY18] R. Connelly, S. Gortler, E. Solomonides, and M. Yampolskaya. Circle packings, triangulations, and rigidity, 2018.
- [CS98] J. Conway and N.J.A. Sloane. *Sphere Packings, Lattices and Groups*. Grundlehren der mathematischen Wissenschaften. Springer New York, 1998.

- [CW10] H. Chang and L. Wang. A Simple Proof of Thue’s Theorem on Circle Packing. *arXiv: Metric Geometry*, 2010.
- [Dev20] The Sage Developers. Sage mathematics software (version 9.0). <http://www.sagemath.org>, 2020.
- [DO11] S. L. Devadoss and J. O’Rourke. *Discrete and Computational Geometry*. Princeton University Press, 2011.
- [Fer19] T. Fernique. A densest ternary circle packing in the plane. <https://arxiv.org/abs/1912.02297>, 2019.
- [Fer22] T. Fernique. Density of binary disc packings: Lower and upper bounds. *Experimental Mathematics*, pages 1–12, 2022.
- [FHS21] T. Fernique, A. Hashemi, and O. Sizova. Compact packings of the plane with three sizes of discs. *Discret. Comput. Geom.*, 66(2):613–635, 2021.
- [FJFS20] E. Fayen, A. Jagannathan, G. Foffi, and F. Smalenburg. Infinite-pressure phase diagram of binary mixtures of (non)additive hard disks. *The Journal of Chemical Physics*, 152(20):204901, 2020.
- [FKS22] S. P. Fekete, P Keldenich, and C. Scheffer. Packing disks into disks with optimal worst-case density. *Discrete and Computational Geometry*, 2022.
- [Flo60] A. Florian. Ausfüllung der Ebene durch Kreise. *Rendiconti del Circolo Matematico di Palermo*, 9:300–312, 1960.
- [FMS17] S. P. Fekete, S. Morr, and C. Scheffer. Split packing: Packing circles into triangles with optimal worst-case density. In *Algorithms and Data Structures*, pages 373–384. Springer International Publishing, 2017.
- [FP21] T. Fernique and D. Pchelina. Compact packings are not always the densest. <https://arxiv.org/abs/2104.12458>, 2021.
- [FT43] L. Fejes Tóth. Über die dichteste Kugellagerung. *Math. Z.*, 48:676–684, 1943.
- [FT84] L. Fejes Tóth. Compact Packing of Circles. *Studia Sci. Math. Hungar.*, 19:103–107, 1984.

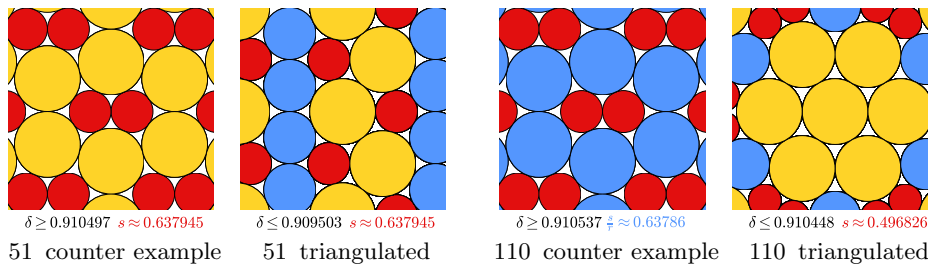
- [FTM58] L. Fejes Tóth and J. Molnár. Unterdeckung und Überdeckung der Ebene durch Kreise. *Mathematische Nachrichten*, 18:235–243, 1958.
- [Gau31] C. F. Gauss. Untersuchungen über die Eigenschaften der positiven ternären quadratischen Formen von Ludwig August Seber. *Göttingische gelehrte Anzeigen*, 1831.
- [HAB⁺17] T. C. Hales, M. Adams, G. Bauer, D. T. Dang, J. Harrison, T. L. Hoang, C. Kaliszyk, V. Magron, S. McLaughlin, T. T. Nguyen, T. Q. Nguyen, T. Nipkow, S. Obua, J. Pleso, J. Rute, A. Solovyev, A. H. T. Ta, T. N. Tran, D. T. Trieu, J. Urban, K. K. Vu, and R. Zunkeller. A formal proof of the Kepler conjecture. *Forum of Mathematics, Pi*, 5:e2, 2017.
- [Hal05] T. C. Hales. A proof of the Kepler conjecture. *Annals of Mathematics*, 162(3):1065–1185, 2005.
- [Hep00] A. Heppes. On the densest packing of discs of radius 1 and $\sqrt{2}-1$. *Studia Scientiarum Mathematicarum Hungarica*, 36:433–454, 2000.
- [Hep03] A. Heppes. Some densest two-size disc packings in the plane. *Discrete and Computational Geometry*, 30:241–262, 2003.
- [HF06] T. C. Hales and S. P. Ferguson. The Kepler conjecture. *Discrete Comput. Geom.*, 36(1):1–269, 2006.
- [HF11] T. C. Hales and S. P. Ferguson. *A Formulation of the Kepler Conjecture*, pages 83–133. Springer New York, New York, NY, 2011.
- [HST12] A. B. Hopkins, F. H. Stillinger, and S. Torquato. Densest binary sphere packings. *Phys. Rev. E*, 85:021130, 2012.
- [Ken05] T Kennedy. A densest compact planar packing with two sizes of discs. <https://arxiv.org/abs/math/0412418>, 2005.
- [Ken06] T. Kennedy. Compact packings of the plane with two sizes of discs. *Discret. Comput. Geom.*, 35(2):255–267, 2006.
- [Lag02] J. Lagarias. Bounds for local density of sphere packings and the Kepler conjecture. *Discrete and Computational Geometry*, 27:165–193, 2002.

- [Mes21] Miek Messerschmidt. The number of configurations of radii that can occur in compact packings of the plane with discs of n sizes is finite. <https://arxiv.org/abs/2110.15831>, 2021.
- [OH11] Patrick I. O’Toole and Toby S. Hudson. New high-density packings of similarly sized binary spheres. *The Journal of Physical Chemistry C*, 115(39):19037–19040, 2011.
- [PDKM15] T. Paik, B. T. Diroll, C. R. Kagan, and C. B. Murray. Binary and Ternary Superlattices Self-Assembled from Colloidal Nanodisks and Nanorods. *Journal of the American Chemical Society*, 137(20):6662–6669, 2015.
- [Thu10] A. Thue. *Über die dichteste Zusammenstellung von kongruenten Kreisen in einer Ebene*. J. Dybwad, 1910.

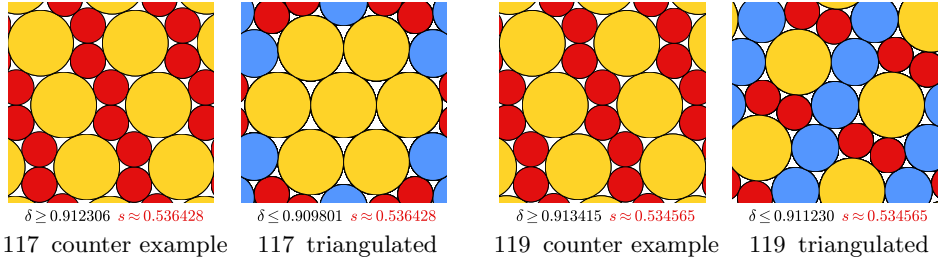
A All counter examples

In this section, we give all the found counter examples grouped by a type of binary triangulated packing we used to construct it (the list of binary triangulated packings is given in Fig. 6). Each counter example is presented as in Fig. 13: to the left, we give the deformed binary packing using a pair of discs whose radii ratio is close to the one of the binary triangulated packing; to the right, the triangulated ternary packings.

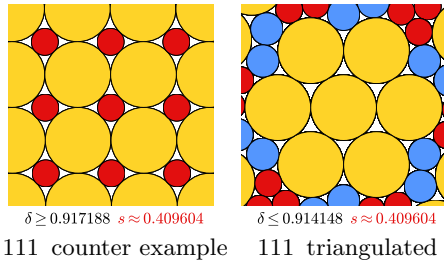
A.1 Counter examples derived from b1



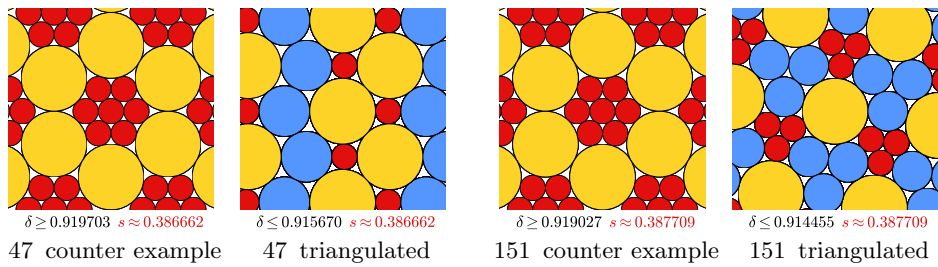
A.2 Counter examples derived from b3



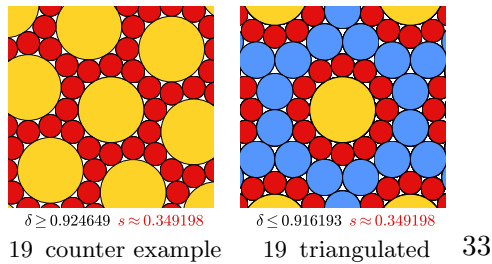
A.3 Counter examples derived from b4

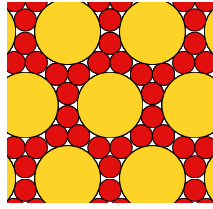


A.4 Counter examples derived from b5



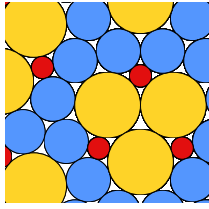
A.5 Counter examples derived from b6





$\delta \geq 0.917953$ $s \approx 0.337336$

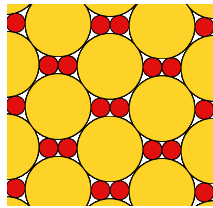
63 counter example



$\delta \leq 0.914301$ $s \approx 0.337336$

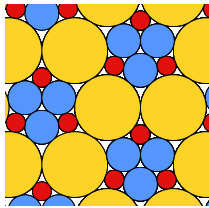
63 triangulated

A.6 Counter examples derived from b7



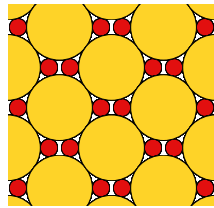
$\delta \geq 0.923787$ $s \approx 0.290478$

60 counter example



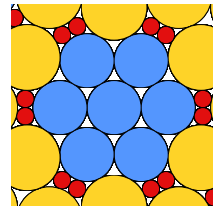
$\delta \leq 0.921391$ $s \approx 0.290478$

60 triangulated



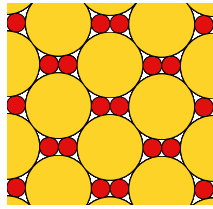
$\delta \geq 0.924545$ $s \approx 0.263654$

73 counter example



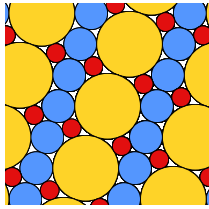
$\delta \leq 0.920565$ $s \approx 0.263654$

73 triangulated



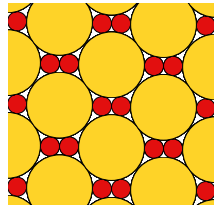
$\delta \geq 0.927652$ $s \approx 0.285714$

64 counter example



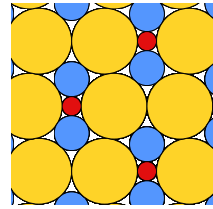
$\delta \leq 0.923712$ $s \approx 0.285714$

64 triangulated



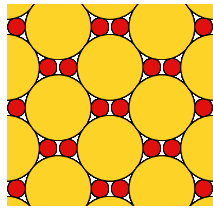
$\delta \geq 0.923374$ $s \approx 0.291004$

80 counter example



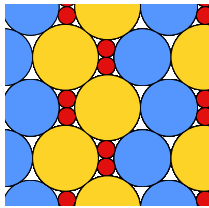
$\delta \leq 0.916939$ $s \approx 0.291004$

80 triangulated



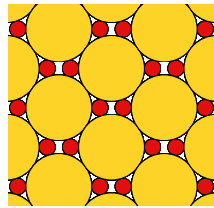
$\delta \geq 0.926300$ $s \approx 0.268266$

70 counter example



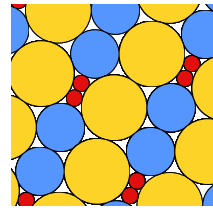
$\delta \leq 0.921134$ $s \approx 0.268266$

70 triangulated



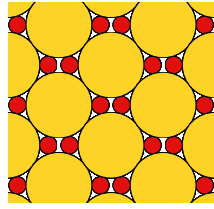
$\delta \geq 0.919930$ $s \approx 0.248062$

95 counter example



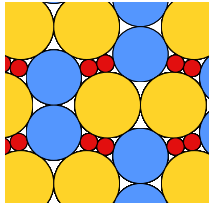
$\delta \leq 0.915309$ $s \approx 0.248062$

95 triangulated



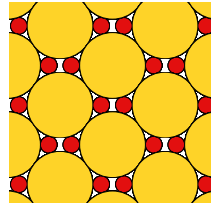
$\delta \geq 0.924033$ $s \approx 0.262214$

98 counter example



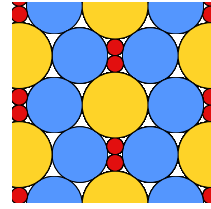
$\delta \leq 0.920708$ $s \approx 0.262214$

98 triangulated



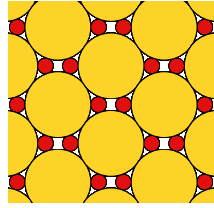
$\delta \geq 0.921070$ $s \approx 0.252651$

139 counter example



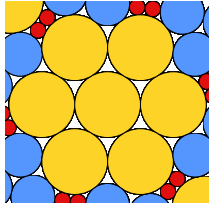
$\delta \leq 0.916585$ $s \approx 0.252651$

139 triangulated



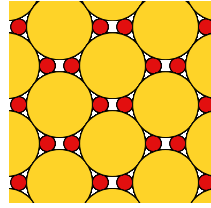
$\delta \geq 0.918039$ $s \approx 0.237538$

99 counter example



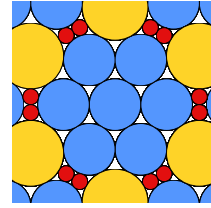
$\delta \leq 0.914656$ $s \approx 0.237538$

99 triangulated



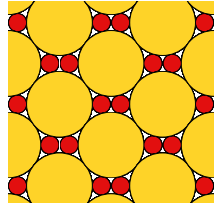
$\delta \geq 0.918420$ $s \approx 0.240205$

142 counter example



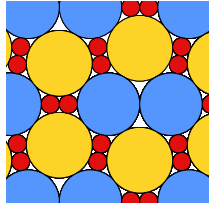
$\delta \leq 0.917352$ $s \approx 0.240205$

142 triangulated



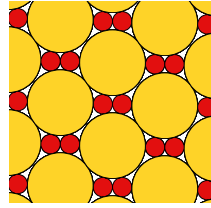
$\delta \geq 0.929245$ $s \approx 0.275178$

104 counter example



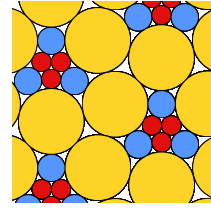
$\delta \leq 0.926316$ $s \approx 0.275178$

104 triangulated



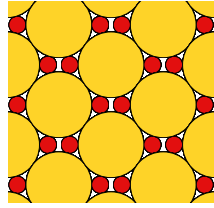
$\delta \geq 0.920311$ $s \approx 0.295016$

152 counter example



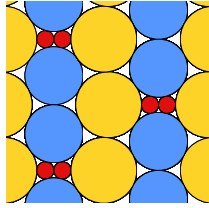
$\delta \leq 0.916740$ $s \approx 0.295016$

152 triangulated



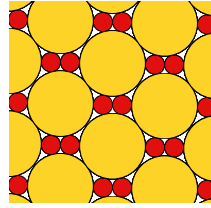
$\delta \geq 0.923104$ $s \approx 0.259471$

133 counter example



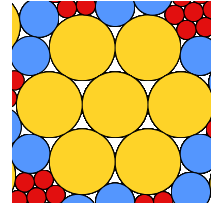
$\delta \leq 0.913852$ $s \approx 0.259471$

133 triangulated



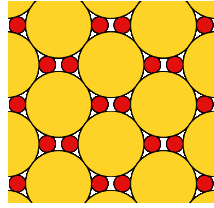
$\delta \geq 0.922609$ $s \approx 0.291987$

154 counter example



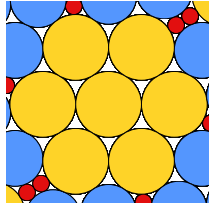
$\delta \leq 0.914322$ $s \approx 0.291987$

154 triangulated



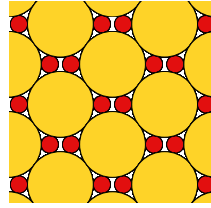
$\delta \geq 0.921135$ $s \approx 0.252889$

137 counter example



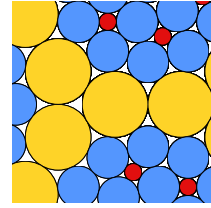
$\delta \leq 0.913256$ $s \approx 0.252889$

137 triangulated



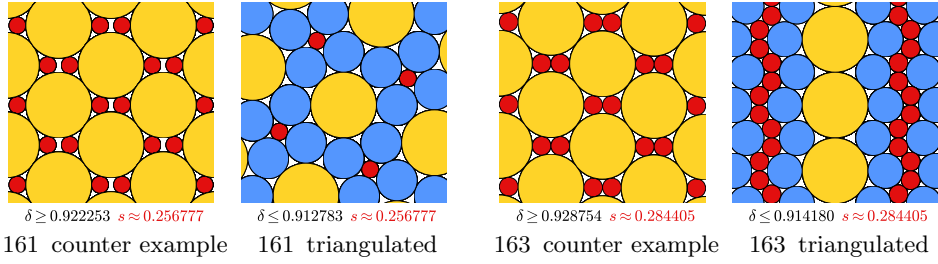
$\delta \geq 0.923895$ $s \approx 0.261820$

159 counter example

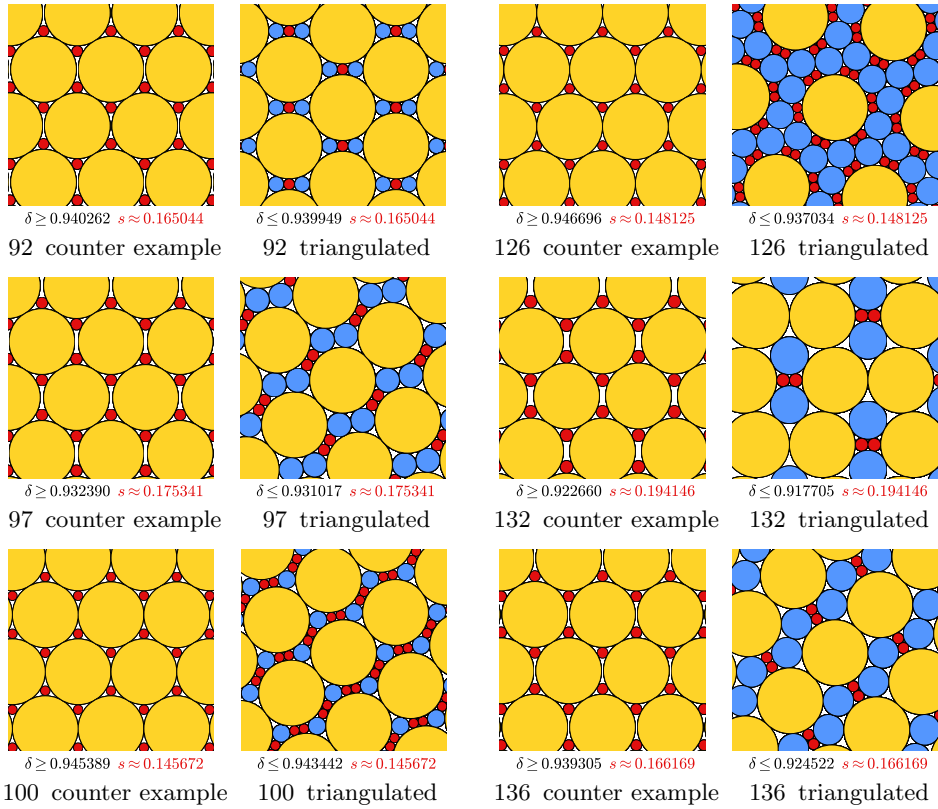


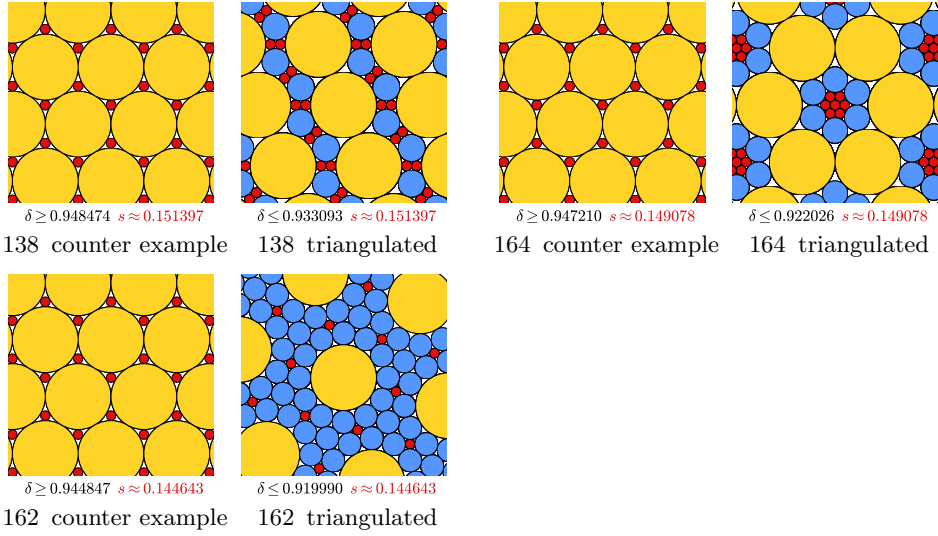
$\delta \leq 0.911735$ $s \approx 0.261820$

159 triangulated



A.7 Counter examples derived from b8





A.8 Counter examples derived from b9

